RAIN: Robotic Task Generalization with Region-Aware Interaction Networks

Anonymous Author

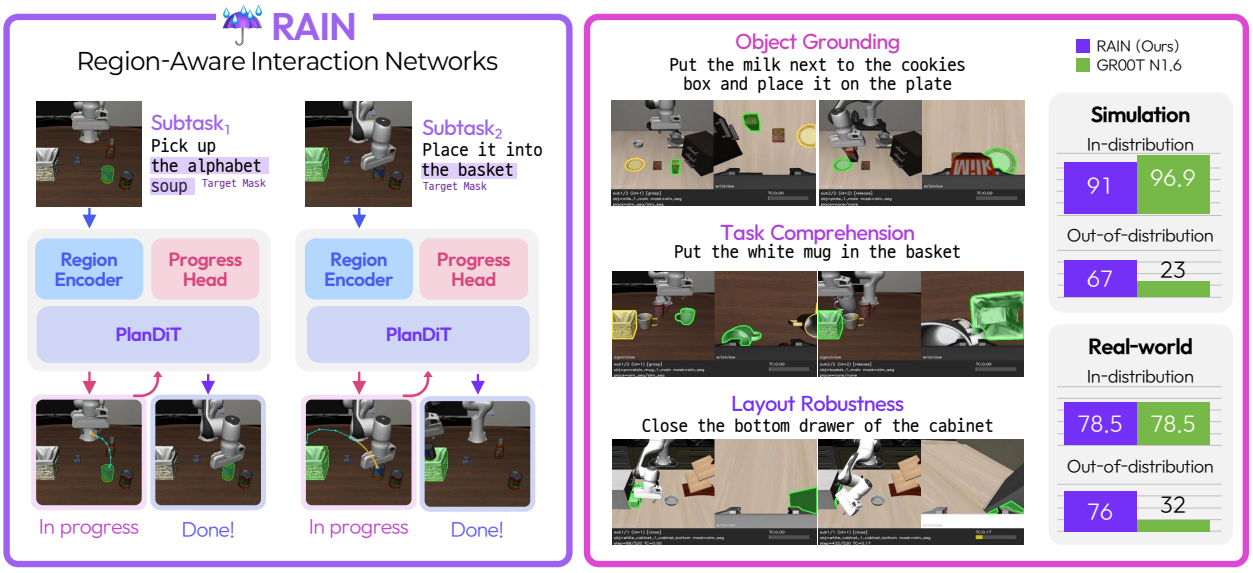

(a) Overview of RAIN (b) Task Generalization

Figure 1: (a) We present **Region-Aware Interaction Networks (RAIN)** that decouples task reasoning from region-aware control by executing each subtask from an action type and target region. (b) Across object grounding, task comprehension, and layout robustness, RAIN shows stronger ID-to-OOD generalization than GR00T N1.6 [26] in simulation and real-world experiments.

Abstract

Existing vision-language-action (VLA) models benefit from broad vision-language priors, but task-specific post-training often couples task reasoning, visual grounding, and control within a single action policy. This coupling encourages policies to memorize execution patterns observed during post-training, causing failures when the task objective remains unchanged but object locations, subtask compositions, or scene layouts change. To address this problem, we propose **Region-Aware Interaction Networks (RAIN)**, an action network that separates task interpretation from region-conditioned execution. Instead of directly mapping a full task instruction and scene to actions, RAIN executes a specified subtask action type on explicit target regions produced by external reasoning and segmentation modules. It conditions multi-view visual features on the target region, exchanges target-aware context across views, predicts target-directed trajectories and actions, and estimates subtask completion to enable automatic subtask transitions. We also introduce a **Reference-based Retargeting Strategy (RRS)**, which synthesizes trajectories for unseen target configurations by smoothly connecting arbitrary initial states to successful reference interactions. Experiments on **LIBERO-EX**, our new LIBERO-derived benchmark for evaluating generalization beyond training task settings, and real-world experiments demonstrate that RAIN generalizes more robustly than existing VLA baselines.

1 Introduction

Robotic manipulation is a central capability for embodied intelligence, with applications spanning industrial automation, household assistance, logistics, and general-purpose service robots. Recent advances in Vision-Language-Models (VLMs) and embodied multimodal models [2, 6, 13, 23, 34], large-scale robot datasets [14, 28, 39], and Vision-Language-Action (VLA) architectures [3, 4, 15, 26, 27, 44] have substantially expanded the range of language-conditioned tasks that robot policies can execute from visual observations. By transferring semantic priors from large multimodal pretraining and visuomotor priors from large robot action corpora, these systems have made general robot policies an increasingly active research direction.

The dominant path toward such policies is to couple pretrained visual-language knowledge with action learning, then post-train the resulting system on the target robot tasks [3, 10, 12, 15, 16, 22, 32, 42, 44]. While this strategy can yield strong performance on post-training tasks, it also creates a critical failure mode: pretrained VLM representations, task semantics, visual grounding, and action generation become optimized around a narrow set of demonstrations. Consequently, a policy that appears competent on the trained tasks can fail under semantics-preserving changes, such as object relocation, subtask recomposition, or scene-layout shifts. This brittleness suggests task memorization rather than task understanding, and recent robustness studies show that high in-distribution VLA performance can collapse under perturbations that preserve task meaning [8, 43]. A robot that truly understands a task should satisfy: (1) *object grounding*, executing the intended interaction even when the referred object moves or a semantically similar unseen object appears; (2) *task comprehension*, executing constituent subtasks of a learned long-horizon task and composing independently learned subtasks into expanded instructions; and (3) *layout robustness*, maintaining the learned interaction under changed scene arrangements. As illustrated in Fig. 1(a), existing post-trained VLAs often degrade sharply when evaluation departs from the training scenario along these axes.

We propose **Region-Aware Interaction Network (RAIN)**, a decoupled framework for robotic task generalization. Given a task description and the current image, a general-purpose VLM independently decomposes the instruction into ordered subtasks and identifies the target object and initial target location for each subtask; A promptable segmentation model such as SAM 2 [36] then converts these decisions into explicit target regions. RAIN learns how to interact with the specified region by combining Target-aware Layer Normalization (TarLN), which conditions each view's visual feature on the target region, a Cross-view Transformer Encoder (CTE), which exchanges information across views and strengthens semantic alignment, and PlanDiT, which predicts a trajectory and action chunk toward the target. A Progress Head further judges at each timestep whether the current subtask has been completed, enabling automatic transition to the next subtask. We also introduce a **Reference-based Retargeting Strategy (RRS)** that synthesizes novel trajectories from arbitrary initial states and smoothly merges them into successful reference interactions. This allows RAIN to learn region-conditioned interactions at target configurations not explicitly covered by demonstrations. By decoupling task reasoning from action post-training, RAIN preserves the general reasoning capability of pretrained VLMs, while improving execution beyond the narrow post-training distribution.

We evaluate RAIN in both simulation and real-world manipulation. In simulation, we train on 40 tasks from LIBERO and construct **LIBERO-EX**, a benchmark designed to evaluate task generalization along object grounding, task comprehension, and layout robustness. Against strong VLA baselines, including OpenVLA-OFT, π_0, $\pi_{0.5}$, and GR00T, RAIN shows stronger generalization on LIBERO-EX while maintaining competitive performance on the original LIBERO suites. We also validate the same design in real-world tabletop manipulation, where RAIN generalizes to changed objects, target locations, subtask combinations, and scene layouts. Our contributions are threefold:

- We propose **RAIN**, a region-aware action model for robotic task generalization that decouples VLM-based task reasoning from post-trained visuomotor control.
- We introduce **RRS**, a reference-based retargeting strategy that synthesizes executable trajectories toward arbitrary target configurations by adapting successful reference interactions.
- We present **LIBERO-EX** and real-world evaluations that test object grounding, task comprehension, and layout robustness, demonstrating that RAIN generalizes more robustly than existing VLA baselines.

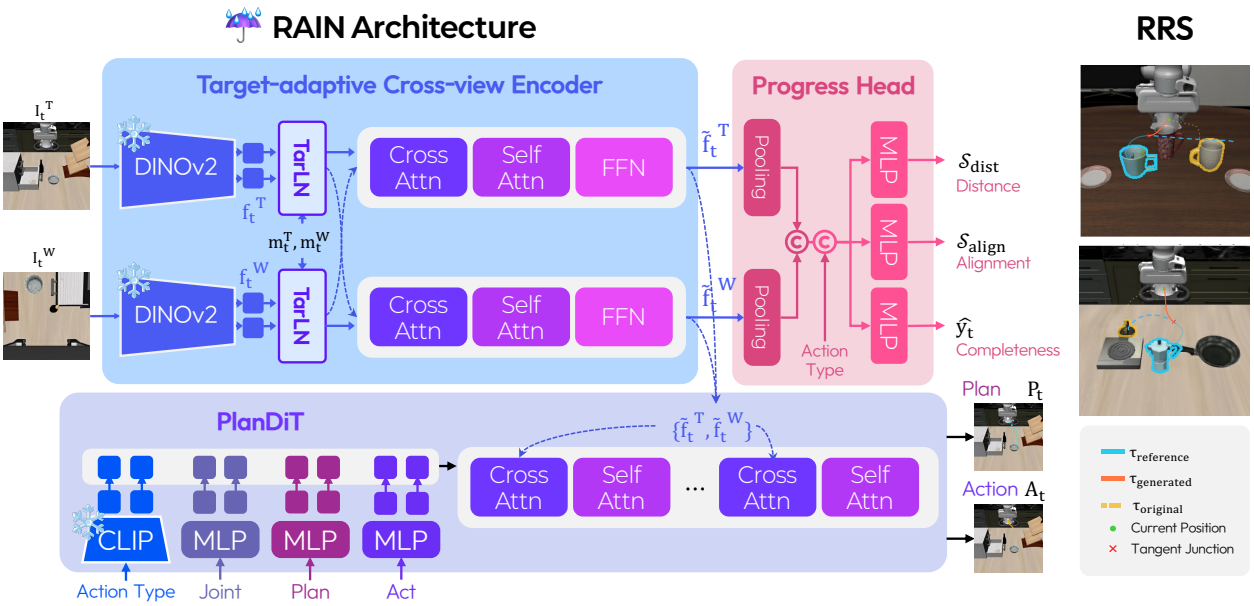

Figure 2: **Overall architecture of RAIN.** For each subtask, RAIN receives an action type and target masks. The **Target-adaptive Cross-view Encoder (TCE)** extracts target-aware features from the third-person and wrist views. The **PlanDiT** jointly predicts future waypoints and action chunks, while the **Progress Head** estimates interaction progress and subtask completion for autonomous transitions. **Reference-based Retargeting strategy (RRS)** augments training by retargeting recorded successful interactions to new target locations with smooth, executable trajectories.

2 Related Works

Vision-Language-Action Models. Vision-language-action (VLA) models [4, 15, 27, 44] have become a major paradigm for language-conditioned robot manipulation by transferring vision-language priors into visuomotor policies. Early systems connected language-conditioned perception with action prediction for real-world control, while open-source generalist policies expanded the setting to broader robot embodiments and task suites. Large robot datasets [14, 28, 39], flow-based policies and generalist robot policies [3, 26], and hierarchical or reasoning-augmented architectures [10, 21, 32, 33, 37, 40] have further extended this paradigm toward longer-horizon and more diverse manipulation tasks. Recent robustness benchmarks such as LIBERO-PRO [43] and LIBERO-Plus [8] show that high in-distribution VLA success can hide memorization, evaluating perturbations to objects, initial states, instructions, layouts, viewpoints, and visual conditions, but largely preserve the original LIBERO task semantics and ask whether the same task remains solvable in a modified but related setup. LIBERO-EX instead targets task-level generalization by evaluating object grounding, task-scope expansion and reduction, and layout robustness on tasks derived from but not identical to the learned LIBERO tasks.

Visual Prompting for Robot Policies. Visual and multimodal prompts provide explicit spatial or procedural information for robot policies. VIMA [11] formulates robot manipulation with multimodal prompts that interleave language and visual tokens. Subsequent work has explored coordinate or sketch-based visual instructions [19, 20], trajectory and trace prompts [42] for spatial-temporal guidance, and pixel-level prompt-native VLA policies [22] that use dense visual cues such as points, lines, boxes, or masks. Visual instruction tuning [23] and pixel grounding [35] provide general vision-language foundations for handling visual prompts and grounded references.

3 Method

In this section, we present Region-Aware Interaction Networks (RAIN), an action network that executes a specified subtask and estimates when the subtask has been completed. As shown in Fig. 2, each subtask is provided as an action type such as *grasp*, *release*, or *open*, together with target masks in the available camera views. In real-world experiments, an external VLM decomposes the task instruction into subtasks before execution and identifies the target object or region for each subtask, while SAM 2 [36] obtains and tracks the corresponding masks. In simulation, action types and target masks are obtained from predefined task annotations. RAIN therefore does not learn the full task description inside the action policy. Instead, it learns how to interact with the specified region by combining target-aware visual encoding, target-directed action generation, and progress estimation.

3.1 Region-Aware Interaction Networks

Although the formulation naturally extends to more camera views, we describe the method with two views for clarity. At each timestep t, RAIN observes two RGB views $\mathcal{I}_t = \{\mathbf{I}_t^T, \mathbf{I}_t^W\}$ from a third-person and wrist camera, the proprioceptive state $\mathbf{q}_t \in \mathbb{R}^7$, an action type c_t, and target masks $\mathcal{M}_t = \{\mathbf{m}_t^T, \mathbf{m}_t^W\}$. The model aims to learn $p(\mathbf{A}_t, \mathbf{P}_t \mid \mathcal{I}_t, \mathbf{q}_t, c_t, \mathcal{M}_t)$, where $\mathbf{A}_t = [\mathbf{a}_t, \ldots, \mathbf{a}_{t+H-1}] \in \mathbb{R}^{H\times 7}$ is an action chunk of horizon H and $\mathbf{P}_t = \{\mathbf{p}_{t,1}, \ldots, \mathbf{p}_{t,N}\} \in \mathbb{R}^{N\times 3}$ is an auxiliary plan with N waypoints. The action chunk contains 3D position, 3D rotation, and gripper commands. The plan represents target-directed 3D waypoints and guides the action decoder toward the region specified by the masks.

RAIN consists of three main components. The Target-adaptive Cross-view Encoder (TCE) extracts target-aware multi-view features from images and masks, the Plan-guided Diffusion Transformer (PlanDiT) predicts the geometric plan and action chunk, and the Progress Head estimates whether the current subtask has been completed.

Target-adaptive Cross-view Encoder. The Target-adaptive Cross-view Encoder (TCE) extracts target-aware representations from both views. Given visual features $\mathbf{f}_t^T, \mathbf{f}_t^W \in \mathbb{R}^{h\times w\times d}$ from a pretrained image encoder, we first resize the target masks to the feature resolution. Target-adaptive Layer Normalization (TarLN) then injects mask information into each view:

$$\mathrm{TarLN}(\mathbf{f}_t^v, \mathbf{m}_t^v) = \gamma^v(\mathbf{m}_t^v) \odot \mathrm{LN}(\mathbf{f}_t^v) + \beta^v(\mathbf{m}_t^v), \quad v \in \{T, W\}. \tag{1}$$

Here, LN denotes layer normalization [1], and $\gamma^v(\cdot), \beta^v(\cdot) \in \mathbb{R}^{h\times w\times d}$ are pixel-wise modulation parameters produced by a spatial MLP, following the spirit of spatially-adaptive normalization [30]. Since both the third-person and wrist views receive their own target masks, the target region is directly injected into each view before cross-view aggregation.

After TarLN, the two views exchange information through cross-view Transformer blocks. Let $\bar{\mathbf{f}}_t^v = \mathrm{TarLN}(\mathbf{f}_t^v, \mathbf{m}_t^v)$. Each block applies cross-attention between the two views, using the first argument as the query and the second as keys and values, followed by self-attention and a feed-forward network:

$$\tilde{\mathbf{f}}_t^T = \mathrm{FFN}(\mathrm{SelfAttn}(\mathrm{CrossAttn}(\bar{\mathbf{f}}_t^T, \bar{\mathbf{f}}_t^W))), \quad \tilde{\mathbf{f}}_t^W = \mathrm{FFN}(\mathrm{SelfAttn}(\mathrm{CrossAttn}(\bar{\mathbf{f}}_t^W, \bar{\mathbf{f}}_t^T))). \tag{2}$$

This design preserves the explicit target conditioning in each view while allowing the wrist and third-person views to share complementary geometric information. We denote the resulting target-aware visual context as $\phi_t = [\tilde{\mathbf{f}}_t^T; \tilde{\mathbf{f}}_t^W]$.

Plan-guided Diffusion Transformer. PlanDiT is a generative Transformer that predicts a target-directed geometric plan and an executable action chunk. The geometric plan $\mathbf{P}_t$ consists of 3D waypoints toward the target region, and the final waypoint $\mathbf{p}_{t,N}$ corresponds to the predicted interaction point. The action chunk $\mathbf{A}_t$ contains the low-level commands executed by the robot controller.

PlanDiT forms an input token sequence $\mathbf{E}_t = [\mathbf{e}_c; \mathbf{e}_q; \mathbf{e}_p; \mathbf{e}_a]$, where $\mathbf{e}_c$ is the action-type embedding, $\mathbf{e}_q$ is the proprioception embedding, and $\mathbf{e}_p, \mathbf{e}_a$ are plan and action tokens embedded from the noisy sample used in flow matching. Transformer blocks process these tokens with cross-attention to the TCE context ϕ_t. To make the action prediction follow the geometric plan, we use an asymmetric self-attention mask: action tokens can attend to plan tokens, but plan tokens cannot attend to action tokens.

We train PlanDiT with Flow Matching [26]. Let $\mathbf{x}_t = [\mathbf{P}_t; \mathbf{A}_t]$ be the concatenated target trajectory. Given a flow step $\tau \in [0, 1]$ and Gaussian noise $\epsilon \sim \mathcal{N}(\mathbf{0}, \mathbf{I})$, we define $\mathbf{x}_t^\tau = \tau \mathbf{x}_t + (1 - \tau)\epsilon$ and optimize the vector field V_θ by

$$\mathcal{L}_{\text{fm}} = \mathbb{E}_{\tau,\epsilon,\mathbf{x}_t} \left[\| V_\theta(\mathbf{x}_t^\tau, \phi_t, \mathbf{q}_t, c_t) - (\mathbf{x}_t - \epsilon) \|_2^2 \right]. \tag{3}$$

We further encourage stable target grounding by enforcing consistency of the final waypoint across frames from the same subtask. Given K sampled frames and the frame t_K closest to completion, we minimize the consistency loss

$$\mathcal{L}_{\text{cons}} = \sum_{k=1}^{K-1} \text{SmoothL1}(\hat{\mathbf{p}}_{t_k,N} - \hat{\mathbf{p}}_{t_K,N}). \tag{4}$$

The total objective for PlanDiT is $\mathcal{L}_{\text{PlanDiT}} = \lambda_{\text{fm}}\mathcal{L}_{\text{fm}} + \lambda_{\text{cons}}\mathcal{L}_{\text{cons}}$, where λ_{fm} and λ_{cons} are loss weights.

Progress Estimation. To autonomously execute multiple subtasks, RAIN uses a Progress Head whose primary role is to decide whether the current subtask has been completed. To support this decision, the head also estimates how far the end-effector remains from the target object and how well the gripper is aligned with the target interaction pose. The head takes the pooled TCE features and the action-type embedding as input and predicts a completion probability $\hat{y}_t$ together with a distance score $\hat{\mathcal{S}}_{\text{dist}}$ and an alignment score $\hat{\mathcal{S}}_{\text{align}}$. The target distance and alignment scores are defined as

$$\mathcal{S}_{\text{dist}} = \exp(-\alpha \|\mathbf{p}_t^{\text{ee}} - \mathbf{p}^g\|_2), \quad \mathcal{S}_{\text{align}} = \frac{1}{2}\left(1 + \frac{\text{tr}((\mathbf{R}_t^{\text{ee}})^\top \mathbf{R}^g) - 1}{2}\right), \tag{5}$$

where $\alpha > 0$ is a scaling constant, $(\mathbf{p}_t^{\text{ee}}, \mathbf{R}_t^{\text{ee}})$ is the current end-effector pose, and $(\mathbf{p}^g, \mathbf{R}^g)$ is the target interaction pose from the demonstration. The completion label y_t is obtained from the annotated subtask boundary. The Progress Head is trained with

$$\mathcal{L}_{\text{head}} = \lambda_{\text{dist}}\mathcal{L}_{\text{dist}} + \lambda_{\text{align}}\mathcal{L}_{\text{align}} + \lambda_{\text{comp}}\mathcal{L}_{\text{comp}}, \tag{6}$$

where $\mathcal{L}_{\text{dist}}$ and $\mathcal{L}_{\text{align}}$ are Smooth L1 losses for the auxiliary progress scores, $\mathcal{L}_{\text{comp}}$ is binary cross entropy between $\hat{y}_t$ and y_t, and $\lambda_{\text{dist}}, \lambda_{\text{align}}, \lambda_{\text{comp}}$ are loss weights. During rollout, RAIN moves to the next subtask when $\hat{y}_t$ exceeds a completion threshold.

3.2 Reference-based Retargeting Strategy

RRS expands region-aware interaction coverage by generating trajectories toward target configurations that are not directly covered by the original demonstrations. Given a recorded reference trajectory $\mathcal{R} = \{\mathbf{r}_0, \ldots, \mathbf{r}_{M-1}\}$ and an arbitrary approach state $\mathbf{x}_0 \in \mathbb{R}^3$ denoting an end-effector position, RRS first identifies a tangent junction $\mathbf{r}_{k^*}$ on the reference trajectory. For each reference point $k \in \{1, \ldots, M-2\}$, we compute the unit tangent vector $\mathbf{t}_k = (\mathbf{r}_{k+1} - \mathbf{r}_{k-1})/\|\mathbf{r}_{k+1} - \mathbf{r}_{k-1}\|_2$, the approach direction $\mathbf{v}_k = (\mathbf{r}_k - \mathbf{x}_0)/\|\mathbf{r}_k - \mathbf{x}_0\|_2$, and the distance $d_k = \|\mathbf{r}_k - \mathbf{x}_0\|_2$. The junction score is

$$S_k = (\mathbf{v}_k^\top \mathbf{t}_k)\left(1 - \frac{d_k}{d_{\max}}\right)\left(1 - \frac{k}{M}\right), \tag{7}$$

and the junction index is selected as $k^* = \arg\max_k S_k$ under proximity and directional-alignment constraints, where $d_{\max}$ is a normalization radius determined by the workspace scale. The first term favors tangential merging into the reference motion, the second avoids long approach paths, and the third preserves as much of the successful reference interaction as possible.

Once the junction is chosen, RRS connects $\mathbf{x}_0$ to $\mathbf{r}_{k^*}$ using a cubic Hermite spline [18]. The variable $u \in [0, 1]$ denotes the normalized interpolation parameter:

$$\mathbf{C}(u) = \psi_{00}(u)\mathbf{x}_0 + \psi_{10}(u)\mathbf{D}_0 + \psi_{01}(u)\mathbf{r}_{k^*} + \psi_{11}(u)\mathbf{D}_1, \quad u \in [0, 1], \tag{8}$$

where $\mathbf{D}_0 = \mathbf{r}_{k^*} - \mathbf{x}_0$, $\mathbf{D}_1 = L\mathbf{t}_{k^*}$, and $L = \|\mathbf{r}_{k^*} - \mathbf{x}_0\|_2$. The basis functions are defined as follows:

$$\psi_{00} = 2u^3 - 3u^2 + 1, \quad \psi_{10} = u^3 - 2u^2 + u, \quad \psi_{01} = -2u^3 + 3u^2, \quad \psi_{11} = u^3 - u^2. \tag{9}$$

Table 1: **Simulation Results on LIBERO and LIBERO-EX.** We report success rates on the original LIBERO suites and our LIBERO-EX task-generalization benchmark. † denotes our reproduction using a single joint 4-suite fine-tuned model trained on all LIBERO suites.

Method	Size	Trainable Params		LIBERO-EX				LIBERO				
		Pre-train	Post-train	Object	Layout	Task	Avg.	Spatial	Object	Goal	Long	Avg.
OpenVLA-OFT [16] [RSS'25]	7B	7B	0.28B	1.6	0.0	0.0	0.5	97.6	98.4	97.9	94.5	97.1
π_0 [3][RSS'25]	3B	3B	3B	38.8	37.2	6.0	27.3	96.8	98.8	95.8	85.2	94.2
π_0 − FAST [31][RSS'25]	3B	3B	3B	0.4	12.8	7.2	6.8	96.4	96.8	88.6	60.2	85.5
$\pi_{0.5}$ [32][CoRL'25]	3B	3B	3B	64.4	57.2	2.4	41.3	98.8	98.2	98.0	92.4	96.9
GR00T N1.6† [26][arXiv'25]	3B	3B	3B	35.2	31.2	2.8	23.0	98.4	99.8	98.0	90.0	95.8
Action-Sketcher [22] [CVPR'26]	3B	3B	3B	47.6	27.6	3.2	26.1	97.2	99.6	94.8	94.8	96.9
Cosmos Policy [17][ICLR'26]	2B	-	2B	40.8	48.4	5.6	31.6	98.1	100.0	98.2	97.6	98.5
SmolVLA [38][arXiv'25]	0.45B	0.1B	0.1B	2.0	6.0	2.0	3.3	90.0	96.0	92.0	71.0	87.3
Dita†[9] [ICCV'25]	0.33B	0.22B	0.22B	29.6	26.0	9.6	21.7	82.0	83.5	80.0	68.5	78.5
RAIN-L (Ours)	**0.62B**	**-**	**0.19B**	**76.0**	**72.0**	**53.2**	**67.0**	**86.8**	**96.0**	**96.0**	**85.2**	**91.0**
RAIN-S (Ours)	**0.25B**	**-**	**0.17B**	**53.6**	**54.0**	**50.4**	**52.7**	**87.8**	**91.4**	**89.8**	**78.4**	**86.9**

Table 2: **Ablation studies on each component of our proposed method.**

(a) CTE

Method	LIBERO
Full model	**91.0**
w/o cross-view	82.1
w/o third mask	86.6
w/o wrist mask	85.8

(b) PlanDiT

Method	LIBERO
Full model	**91.0**
w/o plan token	89.7
w/o $\mathcal{L}_{\text{consis}}$	90.4
w/ bi-directional attn	89.0

(c) Progress head

$\mathcal{L}_{\text{dist}}$	$\mathcal{L}_{\text{align}}$	LIBERO
		89.7
✓		90.5
	✓	89.9
✓	✓	**91.0**

(d) Retarget strategy

Method	LIBERO-EX
no retarget	44.3
linear interp.	58.8
RRS (ours)	**67.0**

The approach segment is discretized with N_{app} steps using $u_i = i/N_{\text{app}}$ for $i = 0, \ldots, N_{\text{app}}$. The final trajectory is obtained by concatenating the generated approach and the remaining reference interaction:

$$\mathcal{P} = [\mathbf{C}(u_0), \ldots, \mathbf{C}(u_{N_{\text{app}}}), \mathbf{r}_{k^*+1}, \ldots, \mathbf{r}_{M-1}]. \tag{10}$$

We convert the approach segment into delta-position actions and interpolate orientation toward the junction pose. After the junction, the recorded reference actions are reused, preserving contact-rich interaction dynamics while exposing RAIN to diverse target locations.

4 Experiments

We evaluate RAIN's task generalization in both simulation and real-world manipulation. In simulation, we compare RAIN with recent state-of-the-art VLA policies on the original LIBERO suites and on LIBERO-EX, a benchmark designed to test generalization beyond the training task settings. In the real world, we evaluate whether the same region-aware action network remains robust under out-of-distribution object, target, and layout changes. Implementation details are provided in Appendix A, with additional simulation and real-world protocols in Appendix B and Appendix C.

4.1 Simulation Experiments

Setting. We train a single policy on the 40 tasks from the LIBERO Spatial, Object, Goal, and Long suites, and compare it with recent VLA models under the same joint-suite evaluation protocol. To evaluate generalization beyond the training distribution, we introduce LIBERO-EX with three categories: object grounding, task comprehension, and layout robustness. Each category contains 25 tasks with 10 evaluation episodes per task. Detailed task definitions and selected initial states are provided in Appendix B and Tables 8–12.

Main results. Tab. 1 compares RAIN with recent VLA models on both LIBERO and LIBERO-EX. Large pretrained baselines often achieve high in-distribution success on LIBERO after post-training, with several

models exceeding 95 average success. However, their performance does not carry over to LIBERO-EX. When the target object, task scope, or scene layout changes, existing VLA policies frequently fail to execute the intended task. The gap is most severe on task comprehension, where all compared baselines remain below 10 success. This split requires policies to execute a constituent subtask of a learned long-horizon task, or to compose learned single-step skills into a new long-horizon task, directly testing whether the policy understands the task structure rather than memorizing a demonstrated sequence. RAIN-L achieves the strongest LIBERO-EX average. RAIN-S, despite using a DINOv2-Small vision encoder and only 0.25B parameters, also surpasses all compared VLA baselines on LIBERO-EX. A per-task breakdown of LIBERO-EX is provided in Tables 5–7.

Ablation study. Tab. 2 analyzes the main components of RAIN. For the Target-adaptive Cross-view Encoder, removing cross-view exchange reduces LIBERO success from 91.0 to 82.1, showing that information exchange around the target object is critical for aligning the third-person and wrist views. Removing either target mask also hurts performance, since the model loses a view-specific visual prompt and becomes more vulnerable to occlusion or viewpoint ambiguity. For PlanDiT, plan tokens improve performance by 1.3 points by predicting a 3D path from the current state toward the target interaction point. The consistency loss $\mathcal{L}_{\text{cons}}$ provides a smaller but consistent gain by aligning the predicted goal of frames from the same subtask. Notably, bi-directional attention between plan and action tokens decreases performance from 91.0 to 89.0, while our asymmetric design lets the plan guide the action without being distorted by action-token noise. The Progress Head benefits from both auxiliary distance and alignment supervision, which help the completion classifier decide when the current subtask is finished. Finally, even without retargeting, RAIN reaches 44.3 on LIBERO-EX, already 3.0 points higher than $\pi_{0.5}$. Linear interpolation from the current gripper state to the goal raises performance to 58.8, while RRS further improves it to 67.0 by generating smoother target-directed interactions.

4.2 Real-World Experiments

Setting. Our real-world platform uses a 6-DoF ROBOTIS OMY-F3M single-arm manipulator with a two-finger gripper. Policies operate through a 7D joint-space action interface and observe robot joint states with RGB images from wrist-mounted, third-person, and top-down cameras. Demonstrations are recorded with a ROS-based system and converted to LeRobot [5]. We evaluate two task families, `Potato-to-Plate` and `Tape-to-Clay`. All policies are trained on the same demonstrations and evaluated under matched robot, camera, action-space, initial-state, and success-criterion settings. We compare with GR00T N1.6 [26], X-VLA [41], and MolmoAct2 [7], using their official codebases with only the interface wrappers required for our robot setup. Detailed setup, split definitions, and baseline training protocols are provided in Appendix C.1–C.4.

Results. As shown in Fig. 3, RAIN maintains stronger out-of-distribution performance across real-world task families. In `Potato-to-Plate`, all methods are trained to place a potato on the middle plate. GR00T N1.6 and MolmoAct2 remain effective when the middle plate changes from round to square, but their success drops sharply when the target plate moves away from the middle position, by 60 and 30 points respectively. RAIN shows little degradation under the same target-location shift, indicating that it follows the specified target region rather than a memorized placement trajectory. In `Tape-to-Clay`, RAIN also achieves the best OOD average, showing robustness to reordered source objects and changed targets. These results support the simulation findings: separating task interpretation from region-conditioned interaction improves generalization when the task semantics are preserved but the visual and spatial context changes.

5 Conclusion

We presented **Region-Aware Interaction Networks (RAIN)**, an action network for robotic task generalization that separates task-level interpretation from region-conditioned execution. Instead of absorbing reasoning, grounding, and control into a single post-trained VLA policy, RAIN receives a subtask action type and an explicit target region from external vision-language reasoning and segmentation models, then learns how to execute the specified interaction. Its target-conditioned multi-view representation, target-directed trajectory and action prediction, and progress estimation enable autonomous subtask transitions

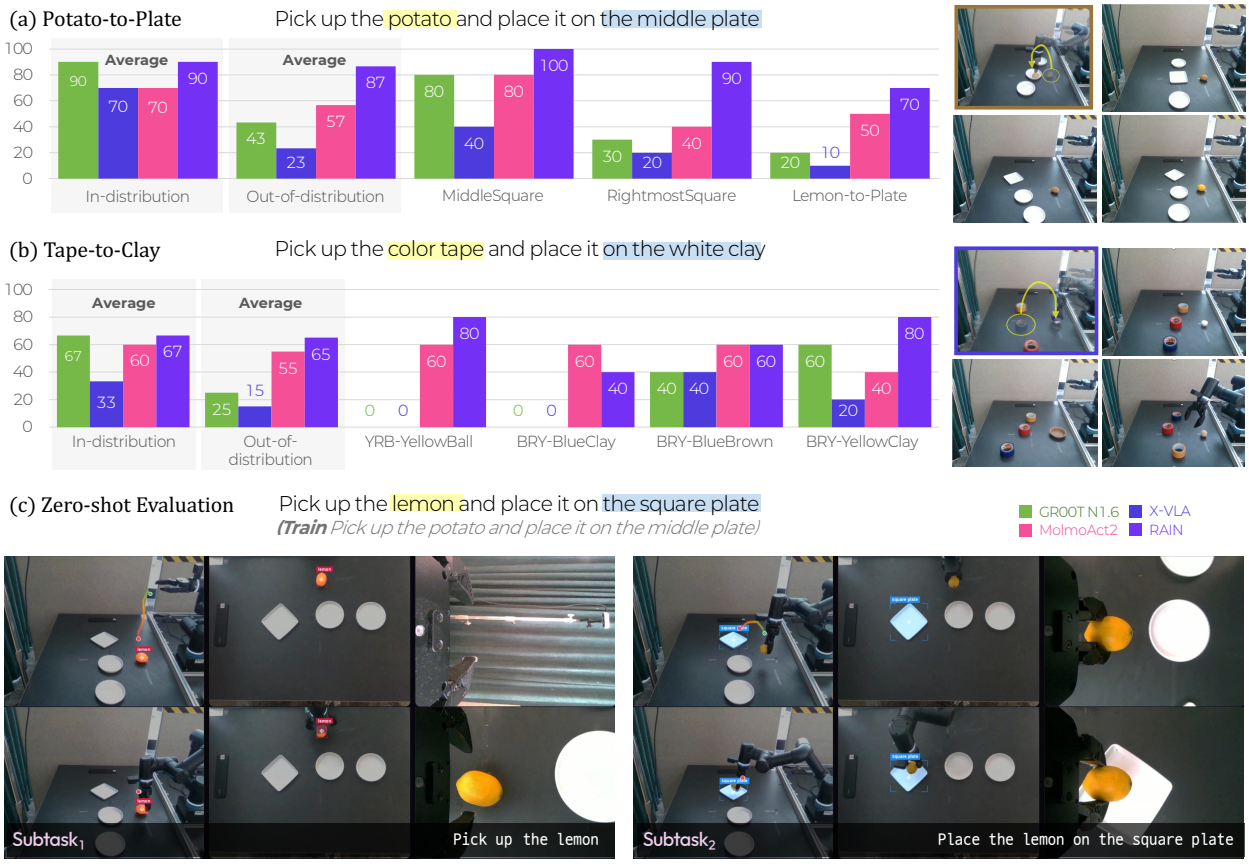

Figure 3: **Real-World Generalization Results.** OOD success rates on **(a)** `Potato-to-Plate` and **(b)** `Tape-to-Clay` task suites, with **(c)** a qualitative zero-shot rollout of RAIN successfully executing the unseen `Lemon-to-Plate` task.

while keeping the action model focused on region-grounded execution. We further introduced **Reference-based Retargeting Strategy (RRS)**, which connects arbitrary target-directed approaches to reference trajectories through tangent junctions, expanding the diversity of region-aware interactions available during training. Experiments on LIBERO-EX and in the real world show that this design improves generalization beyond the post-training task distribution, especially under changes in object placement, task scope, and scene layout.

6 Limitations

RAIN improves task generalization by conditioning action generation on explicit target regions, but this design also makes the policy dependent on reliable visual prompts. When the relevant target region is invisible from all available views, for example due to severe occlusion, poor camera placement, or a target that only becomes visible after substantial scene rearrangement, RAIN may fail because the action model no longer receives a grounded region to interact with. The model can also still fail under extreme out-of-distribution shifts that require interaction geometry or object dynamics far beyond those covered by demonstrations and RRS-generated trajectories. Nevertheless, our results show that separating task interpretation from region-conditioned interaction substantially improves generalization over existing VLA baselines across object grounding, task comprehension, layout robustness, and real-world OOD settings.

References

[1] Jimmy Lei Ba, Jamie Ryan Kiros, and Geoffrey E Hinton. Layer normalization. *arXiv preprint arXiv:1607.06450*, 2016.

[2] Lucas Beyer, Andreas Steiner, Andre Susano Pinto, Alexander Kolesnikov, Xiao Wang, Daniel Salz, Maxim Neumann, Ibrahim Alabdulmohsin, Michael Tschannen, Emanuele Bugliarello, et al. PaliGemma: A versatile 3b VLM for transfer. *arXiv preprint arXiv:2407.07726*, 2024.

[3] Kevin Black, Noah Brown, Danny Driess, Adnan Esmail, Michael Equi, Chelsea Finn, Niccolo Fusai, Lachy Groom, Karol Hausman, Brian Ichter, et al. π_0: A vision-language-action flow model for general robot control. In *Proceedings of Robotics: Science and Systems*, Los Angeles, CA, USA, June 2025. doi: 10.15607/RSS.2025.XXI.010. URL `https://www.roboticsproceedings.org/rss21/p010.html`.

[4] Anthony Brohan, Noah Brown, Justice Carbajal, Yevgen Chebotar, Joseph Dabis, Chelsea Finn, Keerthana Gopalakrishnan, Karol Hausman, Alex Herzog, Jasmine Hsu, et al. RT-1: Robotics transformer for real-world control at scale. In *Proceedings of Robotics: Science and Systems*, Daegu, Republic of Korea, July 2023. doi: 10.15607/RSS.2023.XIX.025. URL `https://www.roboticsproceedings.org/rss19/p025.html`.

[5] Remi Cadene, Simon Alibert, Alexander Soare, Quentin Gallouedec, Adil Zouitine, Steven Palma, Pepijn Kooijmans, Michel Aractingi, Mustafa Shukor, Dana Aubakirova, Martino Russi, Francesco Capuano, Caroline Pascal, Jade Choghari, Jess Moss, and Thomas Wolf. Lerobot: State-of-the-art machine learning for real-world robotics in pytorch. `https://github.com/huggingface/lerobot`, 2024.

[6] Danny Driess, Fei Xia, Mehdi S. M. Sajjadi, Corey Lynch, Aakanksha Chowdhery, Brian Ichter, Ayzaan Wahid, Jonathan Tompson, Quan Vuong, Tianhe Yu, et al. PaLM-E: An embodied multimodal language model. In *Proceedings of the 40th International Conference on Machine Learning*, volume 202 of *Proceedings of Machine Learning Research*, pages 8469–8488. PMLR, 2023.

[7] Haoquan Fang, Jiafei Duan, Donovan Clay, Sam Wang, Shuo Liu, Weikai Huang, Xiang Fan, Wei-Chuan Tsai, Shirui Chen, Yi Ru Wang, et al. Molmoact2: Action reasoning models for real-world deployment. *arXiv preprint arXiv:2605.02881*, 2026.

[8] Senyu Fei, Siyin Wang, Junhao Shi, Zihao Dai, Jikun Cai, Pengfang Qian, Li Ji, Xinzhe He, Shiduo Zhang, Zhaoye Fei, et al. Libero-plus: In-depth robustness analysis of vision-language-action models. *arXiv preprint arXiv:2510.13626*, 2025.

[9] Zhi Hou, Tianyi Zhang, Yuwen Xiong, Haonan Duan, Hengjun Pu, Ronglei Tong, Chengyang Zhao, Xizhou Zhu, Yu Qiao, Jifeng Dai, et al. Dita: Scaling diffusion transformer for generalist vision-language-action policy. In *Proceedings of the IEEE/CVF International Conference on Computer Vision*, pages 7686–7697, 2025.

[10] Chi-Pin Huang, Yueh-Hua Wu, Min-Hung Chen, Yu-Chiang Frank Wang, and Fu-En Yang. Thinkact: Vision-language-action reasoning via reinforced visual latent planning. *arXiv preprint arXiv:2507.16815*, 2025.

[11] Yunfan Jiang, Agrim Gupta, Zichen Zhang, Guanzhi Wang, Yongqiang Dou, Yanjun Chen, Li Fei-Fei, Anima Anandkumar, Yuke Zhu, and Linxi Fan. Vima: General robot manipulation with multimodal prompts. In *Fortieth International Conference on Machine Learning*, 2023.

[12] Gi-Cheon Kang, Junghyun Kim, Kyuhwan Shim, Jun Ki Lee, and Byoung-Tak Zhang. Clip-rt: Learning language-conditioned robotic policies from natural language supervision. *arXiv preprint arXiv:2411.00508*, 2024.

[13] Siddharth Karamcheti, Suraj Nair, Ashwin Balakrishna, Percy Liang, Thomas Kollar, and Dorsa Sadigh. Prismatic VLMs: Investigating the design space of visually-conditioned language models. In *Proceedings of the 41st International Conference on Machine Learning*, volume 235 of *Proceedings of Machine Learning Research*, pages 23123–23144. PMLR, 2024.

[14] Alexander Khazatsky, Karl Pertsch, Suraj Nair, Ashwin Balakrishna, Sudeep Dasari, Siddharth Karamcheti, Soroush Nasiriany, Mohan Kumar Srirama, Lawrence Yunliang Chen, Kirsty Ellis, et al. DROID: A large-scale in-the-wild robot manipulation dataset. In *Proceedings of Robotics: Science and Systems*, Delft, Netherlands, July 2024. doi: 10.15607/RSS.2024.XX.120. URL `https://www.roboticsproceedings.org/rss20/p120.html`.

[15] Moo Jin Kim, Karl Pertsch, Siddharth Karamcheti, Ted Xiao, Ashwin Balakrishna, Suraj Nair, Rafael Rafailov, Ethan Foster, Grace Lam, Pannag Sanketi, Quan Vuong, Thomas Kollar, Benjamin Burchfiel, Russ Tedrake, Dorsa Sadigh, Sergey Levine, Percy Liang, and Chelsea Finn. Openvla: An open-source vision-language-action model. In *Conference on Robot Learning*, 2024. URL `https://openreview.net/forum?id=ZMnD6QZAE6`.

[16] Moo Jin Kim, Chelsea Finn, and Percy Liang. Fine-tuning vision-language-action models: Optimizing speed and success. In *Proceedings of Robotics: Science and Systems*, Los Angeles, CA, USA, June 2025. doi: 10.15607/RSS.2025.XXI.017.

[17] Moo Jin Kim, Yihuai Gao, Tsung-Yi Lin, Yen-Chen Lin, Yunhao Ge, Grace Lam, Percy Liang, Shuran Song, Ming-Yu Liu, Chelsea Finn, and Jinwei Gu. Cosmos policy: Fine-tuning video models for visuomotor control and planning. *arXiv preprint arXiv:2601.16163*, 2026.

[18] Doris HU Kochanek and Richard H Bartels. Interpolating splines with local tension, continuity, and bias control. In *Proceedings of the 11th annual conference on Computer graphics and interactive techniques*, pages 33–41, 1984.

[19] Xiang Li, Cristina Mata, Jongwoo Park, Kumara Kahatapitiya, Yoo Sung Jang, Jinghuan Shang, Kanchana Ranasinghe, Ryan Burgert, Mu Cai, Yong Jae Lee, et al. Llara: Supercharging robot learning data for vision-language policy. *arXiv preprint arXiv:2406.20095*, 2024.

[20] Yanbang Li, Ziyang Gong, Haoyang Li, Xiaoqi Huang, Haolan Kang, Guangping Bai, and Xianzheng Ma. Robotic visual instruction. In *Proceedings of the Computer Vision and Pattern Recognition Conference*, pages 12155–12165, 2025.

[21] Yi Li, Yuquan Deng, Jesse Zhang, Joel Jang, Marius Memmel, Raymond Yu, Caelan Reed Garrett, Fabio Ramos, Dieter Fox, Anqi Li, et al. Hamster: Hierarchical action models for open-world robot manipulation. *arXiv preprint arXiv:2502.05485*, 2025.

[22] Wenqi Liang, Gan Sun, Yao He, Jiahua Dong, Suyan Dai, Ivan Laptev, Salman Khan, and Yang Cong. Pixelvla: Advancing pixel-level understanding in vision-language-action model. In *International Conference on Learning Representations*, 2026. URL `https://openreview.net/forum?id=7M6ryCABIc`.

[23] Haotian Liu, Chunyuan Li, Qingyang Wu, and Yong Jae Lee. Visual instruction tuning. In A. Oh, T. Naumann, A. Globerson, K. Saenko, M. Hardt, and S. Levine, editors, *Advances in Neural Information Processing Systems*, volume 36, pages 34892–34916. Curran Associates, Inc., 2023. URL `https://proceedings.neurips.cc`.

[24] Ilya Loshchilov and Frank Hutter. Decoupled weight decay regularization. *arXiv preprint arXiv:1711.05101*, 2017.

[25] NVIDIA. Cosmos-reason2: Physical ai common sense and embodied reasoning models. `https://huggingface.co/nvidia/Cosmos-Reason2-2B`, 2026. Model card.

[26] NVIDIA, Johan Bjorck, Fernando Castañeda, Nikita Cherniadev, Xingye Da, Runyu Ding, Linxi Fan, Yu Fang, Dieter Fox, Fengyuan Hu, Spencer Huang, et al. GR00T N1: An open foundation model for generalist humanoid robots. *arXiv preprint arXiv:2503.14734*, 2025.

[27] Octo Model Team, Dibya Ghosh, Homer Walke, Karl Pertsch, Kevin Black, Oier Mees, Sudeep Dasari, Joey Hejna, Charles Xu, Jianlan Luo, Tobias Kreiman, You Liang Tan, Lawrence Yunliang Chen, Pannag Sanketi, Quan Vuong, Ted Xiao, Dorsa Sadigh, Chelsea Finn, and Sergey Levine. Octo: An open-source generalist robot policy. In *Proceedings of Robotics: Science and Systems*, Delft, Netherlands, 2024.

[28] Abby O'Neill, Abdul Rehman, Abhiram Maddukuri, Abhishek Gupta, Abhishek Padalkar, Abraham Lee, Acorn Pooley, Agrim Gupta, Ajay Mandlekar, Ajinkya Jain, et al. Open X-Embodiment: Robotic learning datasets and RT-X models. In *2024 IEEE International Conference on Robotics and Automation (ICRA)*, pages 6892–6903. IEEE, 2024.

[29] Maxime Oquab, Timothée Darcet, Théo Moutakanni, Huy Vo, Marc Szafraniec, Vasil Khalidov, Pierre Fernandez, Daniel Haziza, Francisco Massa, Alaaeldin El-Nouby, et al. Dinov2: Learning robust visual features without supervision. *arXiv preprint arXiv:2304.07193*, 2023.

[30] Taesung Park, Ming-Yu Liu, Ting-Chun Wang, and Jun-Yan Zhu. Semantic image synthesis with spatially-adaptive normalization. In *Proceedings of the IEEE/CVF conference on computer vision and pattern recognition*, pages 2337–2346, 2019.

[31] Karl Pertsch, Kyle Stachowicz, Brian Ichter, Danny Driess, Suraj Nair, Quan Vuong, Oier Mees, Chelsea Finn, and Sergey Levine. Fast: Efficient action tokenization for vision-language-action models. *arXiv preprint arXiv:2501.09747*, 2025.

[32] Physical Intelligence, Kevin Black, Noah Brown, James Darpinian, Karan Dhabalia, Danny Driess, Adnan Esmail, Michael Equi, Chelsea Finn, Niccolo Fusai, et al. $pi_0.5$: a vision-language-action model with open-world generalization. *arXiv preprint arXiv:2504.16054*, 2025.

[33] Delin Qu, Haoming Song, Qizhi Chen, Yuanqi Yao, Xinyi Ye, Yan Ding, Zhigang Wang, JiaYuan Gu, Bin Zhao, Dong Wang, et al. Spatialvla: Exploring spatial representations for visual-language-action model. *arXiv preprint arXiv:2501.15830*, 2025.

[34] Alec Radford, Jong Wook Kim, Chris Hallacy, Aditya Ramesh, Gabriel Goh, Sandhini Agarwal, Girish Sastry, Amanda Askell, Pamela Mishkin, Jack Clark, et al. Learning transferable visual models from natural language supervision. In *Proceedings of the 38th International Conference on Machine Learning*, volume 139 of *Proceedings of Machine Learning Research*, pages 8748–8763. PMLR, 2021.

[35] Hanoona Rasheed, Muhammad Maaz, Sahal Shaji, Abdelrahman Shaker, Salman Khan, Hisham Cholakkal, Rao M. Anwer, Eric Xing, Ming-Hsuan Yang, and Fahad S. Khan. Glamm: Pixel grounding large multimodal model. *The IEEE/CVF Conference on Computer Vision and Pattern Recognition*, 2024.

[36] Nikhila Ravi, Valentin Gabeur, Yuan-Ting Hu, Ronghang Hu, Chaitanya Ryali, Tengyu Ma, Haitham Khedr, Roman Rädle, Chloe Rolland, Laura Gustafson, et al. Sam 2: Segment anything in images and videos. *arXiv preprint arXiv:2408.00714*, 2024.

[37] Lucy Xiaoyang Shi, Brian Ichter, Michael Equi, Liyiming Ke, Karl Pertsch, Quan Vuong, James Tanner, Anna Walling, Haohuan Wang, Niccolo Fusai, et al. Hi robot: Open-ended instruction following with hierarchical vision-language-action models. *arXiv preprint arXiv:2502.19417*, 2025.

[38] Mustafa Shukor, Dana Aubakirova, Francesco Capuano, Pepijn Kooijmans, Steven Palma, Adil Zouitine, Michel Aractingi, Caroline Pascal, Martino Russi, Andres Marafioti, et al. Smolvla: A vision-language-action model for affordable and efficient robotics. *arXiv preprint arXiv:2506.01844*, 2025.

[39] Homer Rich Walke, Kevin Black, Tony Z. Zhao, Quan Vuong, Chongyi Zheng, Philippe Hansen-Estruch, Andre Wang He, Vivek Myers, Moo Jin Kim, Max Du, Abraham Lee, Kuan Fang, Chelsea Finn, and Sergey Levine. Bridgedata v2: A dataset for robot learning at scale. In *Proceedings of The 7th Conference on Robot Learning*, volume 229 of *Proceedings of Machine Learning Research*, pages 1723–1736. PMLR, 2023.

[40] Michał Zawalski, William Chen, Karl Pertsch, Oier Mees, Chelsea Finn, and Sergey Levine. Robotic control via embodied chain-of-thought reasoning. *arXiv preprint arXiv:2407.08693*, 2024.

[41] Jinliang Zheng, Jianxiong Li, Zhihao Wang, Dongxiu Liu, Xirui Kang, Yuchun Feng, Yinan Zheng, Jiayin Zou, Yilun Chen, Jia Zeng, et al. X-vla: Soft-prompted transformer as scalable cross-embodiment vision-language-action model. *arXiv preprint arXiv:2510.10274*, 2025.

[42] Ruijie Zheng, Yongyuan Liang, Shuaiyi Huang, Jianfeng Gao, Hal Daumé III, Andrey Kolobov, Furong Huang, and Jianwei Yang. Tracevla: Visual trace prompting enhances spatial-temporal awareness for generalist robotic policies. *arXiv preprint arXiv:2412.10345*, 2024.

[43] Xueyang Zhou, Yangming Xu, Guiyao Tie, Yongchao Chen, Guowen Zhang, Duanfeng Chu, Pan Zhou, and Lichao Sun. Libero-pro: Towards robust and fair evaluation of vision-language-action models beyond memorization. *arXiv preprint arXiv:2510.03827*, 2025.

[44] Brianna Zitkovich, Tianhe Yu, Sichun Xu, Peng Xu, Ted Xiao, Fei Xia, Jialin Wu, Paul Wohlhart, Stefan Welker, Ayzaan Wahid, et al. RT-2: Vision-language-action models transfer web knowledge to robotic control. In *Proceedings of The 7th Conference on Robot Learning*, volume 229 of *Proceedings of Machine Learning Research*, pages 2165–2183. PMLR, 2023.

Appendix

A Implementation Details

Table 3: **Backbone and model configurations.** We use frozen DINOv2 image encoders and frozen CLIP text encoders for RAIN-L and RAIN-S.

Item	**RAIN-L**	**RAIN-S**
DINO backbone	DINOv2-L/14	DINOv2-S/14
CLIP text encoder	ViT-L/14	ViT-B/32
DINO token dim	1024	384
CLIP token dim	768	512
Hidden dim	1024	768
DiT blocks / heads	12 / 12	12 / 12

Model architecture. RAIN uses DINOv2 [29] as the vision encoder and CLIP [34] as the text encoder, both frozen during training. RAIN-L uses DINOv2 ViT-L/14 and CLIP ViT-L/14, while RAIN-S uses DINOv2 ViT-S/14 and CLIP ViT-B/32; detailed dimensions are summarized in Tab. 3. The Target-adaptive Cross-view Encoder (TCE) uses a single cross-view Transformer block composed of cross-attention, self-attention, and a feed-forward network. When three views are available, each view is used as the query and the concatenation of the other two views is used as the key and value for cross-attention. PlanDiT consists of 12 Transformer layers. We set the action chunk size to 16 and the plan token length to 8 during training. During rollout, PlanDiT uses 4 diffusion steps and the controller executes the first 8 actions from each predicted chunk.

Training. All models are trained with a batch size of 1024 for 100k iterations using AdamW [24] with a base learning rate of 1×10^{-4}. We use linear warmup for the first 2,000 steps followed by a cosine decay schedule. For stable optimization, we use mixed-precision training and gradient clipping with threshold 1.0. Training follows a two-stage procedure: we first train all modules except the Progress Head, then freeze all other parameters and train the Progress Head. The loss weights are set empirically to $\lambda_{\text{fm}} = 1.0$, $\lambda_{\text{cons}} = 0.1$, $\lambda_{\text{dist}} = 0.3$, $\lambda_{\text{align}} = 0.3$, and $\lambda_{\text{comp}} = 1.2$. All experiments are run on 4 NVIDIA B200 GPUs.

Retarget augmentation. Our retarget augmentation reconstructs future interactions from the same demonstration episode at the current observation timestep. Importantly, it does not create arbitrary cross-episode combinations; candidates are restricted to future subtasks that can be executed immediately from the current state. We only sample subtasks that occur after the current subtask, never past subtasks or subtasks from other episodes, and do not use reverse augmentation in our experiments. We estimate the current hand state and filter candidates by action type: an empty hand permits *grasp* and *close*, while an object-holding hand permits *release* and *close*. This prevents physically invalid retargets such as releasing without a held object or grasping a new object while already holding one. To avoid trivial continuation of the original task, we also exclude the original task-completion edge. In particular, release retargeting does not reuse the current subtask's original place target. For example, *grasp mug* followed by *place mug in microwave* is treated as

Table 4: **Dita LIBERO fine-tuning and reproduction details.** The official Dita recipe reports LIBERO suite results from the released method, while Dita† denotes our single joint 4-suite fine-tuning reproduction. Both use the standard LIBERO suites (Spatial, Object, Goal, Long) and exclude LIBERO-90. – denotes not applicable / not reported.

Setting	**Dita official recipe**	**Dita† reproduction**
Base & shared settings		
Base model	Dita-0.33B	Dita-0.33B
Parameters	334M total / 221M trainable	334M total / 221M trainable
Text encoder	Frozen CLIP text encoder	Frozen CLIP text encoder
Vision backbone	DINOv2, 224×224	DINOv2, 224×224
Visual reducer	Q-Former, depth 4, 32 tokens	Q-Former, depth 4, 32 tokens
Policy backbone	LLaMA2-style Transformer, 12 layers, hidden 768	LLaMA2-style Transformer, 12 layers, hidden 768
Action decoder	DDPM diffusion head	DDPM diffusion head
DDPM train steps	100	100
Inference steps	10	10
Action chunk	10	10
Action dim.	7	7
Optimizer	AdamW	AdamW
Image augmentation	yes	yes
Training recipe		
Fine-tuning scheme	Suite-specific FT	Single joint 4-suite FT
Training suites	Spatial/Object/Goal/Long	Spatial, Object, Goal, Long
Excluded suite	LIBERO-90	LIBERO-90
Dataset name	`libero_{spatial,object,goal,10}_no_noops`	`libero_all_no_noops`
Dataset mixture	–	Four no-noops RLDS datasets, weight 1.0 each
Base checkpoint	`dit_policy_checkpoint.pth`	`dit_policy_checkpoint.pth`
Finetune scope	Full FT except CLIP text encoder	Full FT except CLIP text encoder
# GPUs	8	8
Batch size / GPU	64	16
Effective batch size	512	128
Learning rate	1e−4; Long uses 5e−4	1e−4

the original task progression, whereas *holding mug* followed by *close microwave door* is a valid retarget candidate.

Candidates are further filtered by visual and geometric validity. A future target must have a valid target mask, its mask must not overlap too heavily with the current object mask, and the target interaction point must be sufficiently far from the current end-effector pose. We use a minimum distance threshold of 3 cm to avoid near-duplicate state copies. For release retargeting, we do not copy the source object of the future subtask; instead, the current held object is paired with the future place target. This defines release retargets as interactions between the held object and a feasible future placement region, enabling combinations such as placing a held white mug on a future right plate.

Observation and deployment setup. In LIBERO simulation, images are resized to 224×224 and RAIN uses two views: agent view and wrist view. We use the object IDs and segmentation masks provided by the LIBERO simulator for both views. In real-world experiments, images are resized to 336×336 and RAIN uses three views: top view, third-person view, and wrist view. A Cosmos-Reason2-2B model [25] decomposes each task into subtasks and predicts the initial target bounding box; SAM 2 [36] then tracks real-time masks for the top and third-person views, while the wrist view is used as an RGB observation without a mask. During multi-subtask execution, the Progress Head marks the current subtask as completed when its completion score exceeds 0.7 for two consecutive timesteps, after which the policy switches to the next subtask.

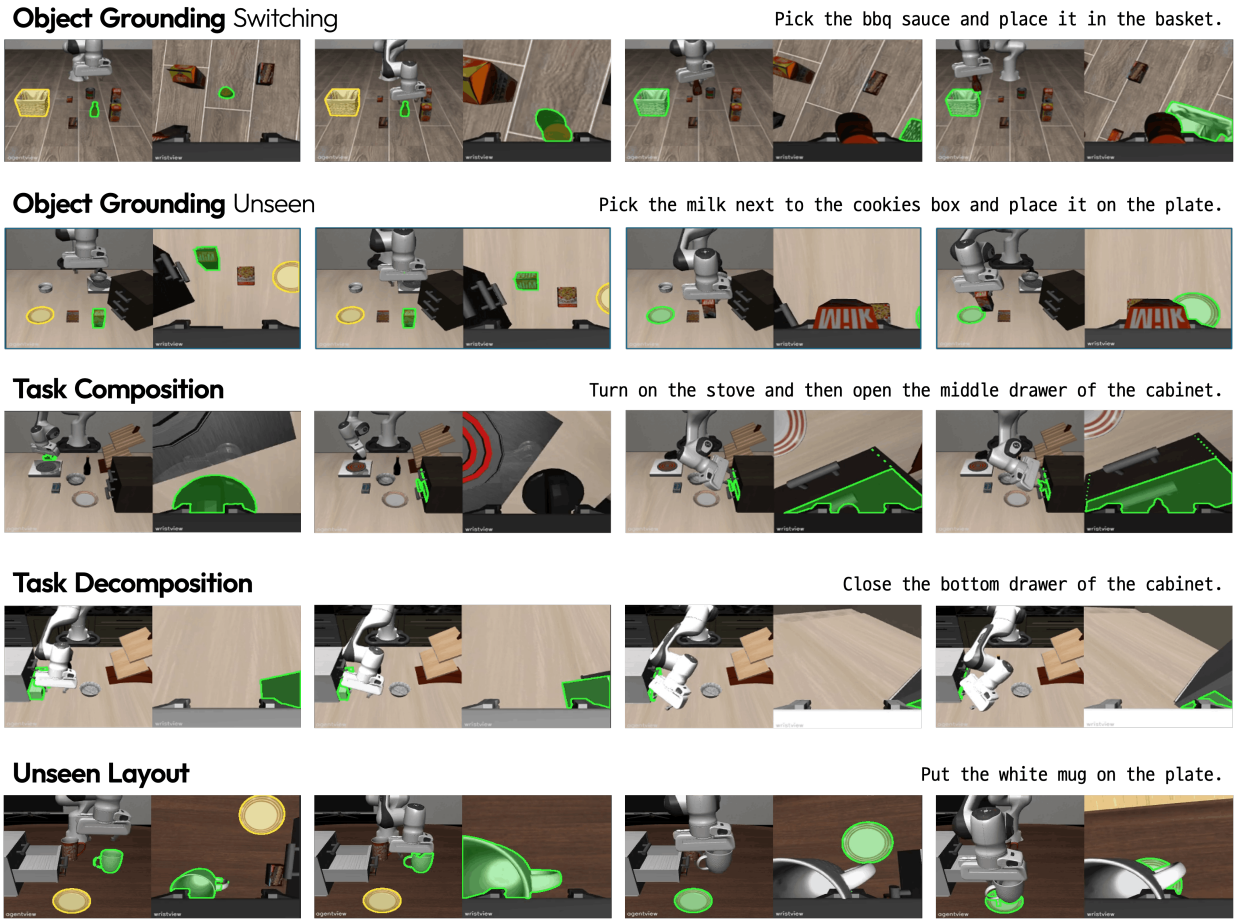

Figure 4: **Qualitative results on LIBERO-EX.**

B Simulation Experiment Details

B.1 Finetuning of Baseline Model on LIBERO

Standard LIBERO recipes are typically optimized for suite-specific performance, reporting results using separate fine-tuned checkpoints for each individual suite (i.e., LIBERO-Spatial, Object, Goal, and Long). To evaluate a model's capacity to absorb the entire distribution of standard tasks within a single policy, we reproduce representative baseline methods under a joint 4-suite fine-tuning protocol. Our reproduction strictly adheres to the officially released training codes and configurations, with the sole modification being the dataset mixture to train a single checkpoint on the union of all four standard suites. Specifically, for Dita [9] and GR00T N1.6 [26], we strictly follow the hyperparameter settings and optimization pipelines provided in their respective official repositories, ensuring a faithful reproduction under the combined multi-suite data distribution.

B.2 LIBERO-EX

LIBERO-EX is derived from LIBERO to evaluate whether a policy trained on the original LIBERO tasks can generalize beyond the exact task settings seen during post-training. We organize LIBERO-EX into three splits, *object*, *layout*, and *task*, corresponding to object grounding, layout robustness, and task comprehension. Each split contains 25 tasks and each task is evaluated over 10 episodes. The task definitions and selected initial observations are shown in Tab. 8–Tab. 12, and detailed per-task success rates corresponding to Tab. 1 are reported in Tab. 5–Tab. 7. We also provide qualitative results of RAIN in Fig. 4.

Object grounding. The object split tests whether a policy can ground the intended object rather than replaying a scene-specific trajectory. It contains two types of tasks. *Unseen object* tasks preserve the learned task structure but require interaction with objects that did not appear in the corresponding training scene. *Object switching* tasks use familiar scenes but swap the positions of multiple objects, forcing the policy to select the instruction-relevant object under changed spatial assignments. As shown in Tab. 5, RAIN-L achieves 76.0 average success, outperforming the strongest baseline $\pi_{0.5}$ by 11.6 points.

Layout robustness. The layout split changes the scene composition of learned tasks by rearranging objects and adding distractors. Compared with object grounding, this split introduces more aggressive visual and geometric changes because the relevant object must be identified and manipulated in a scene whose overall arrangement differs from training. Several baselines struggle under this shift: Action-Sketcher drops from 47.6 on object grounding to 27.6 on layout robustness, GR00T N1.6 reaches only 31.2, and Dita reaches 26.0. In contrast, RAIN-L maintains similar performance across the two splits, achieving 76.0 on object grounding and 72.0 on layout robustness. Per-task results are provided in Tab. 6.

Task comprehension. The task split evaluates whether a policy understands the structure of a task rather than memorizing the demonstrated sequence. It consists of *task decomposition*, where a policy trained on a long-horizon task must execute only the requested constituent subtask, and *task composition*, where independently learned single-step tasks are combined into a new long-horizon instruction. For decomposition tasks, completing the original full long-horizon task instead of the requested subtask is counted as failure. As shown in Tab. 7, most VLA baselines fail on this split, with all compared baselines below 10 average success. In particular, task composition is rarely solved, indicating that existing policies heavily rely on memorized post-training trajectories rather than compositional task understanding. RAIN-L and RAIN-S substantially improve this split, achieving 53.2 and 50.4 average success, respectively.

Table 5: **Detailed LIBERO-EX Object Grounding Results.** Each column is a LIBERO-EX task index from the task-definition tables above. Success rates are reported in % over 10 evaluation episodes, with the category average in the last column.

Model	**Task ID**																									**Avg.**
	001	002	003	004	005	006	007	008	009	010	011	012	013	014	015	016	017	018	019	020	021	022	023	024	025	Avg.
OpenVLA-OFT	0	0	0	0	40	0	0	0	0	0	0	0	0	0	0	0	0	0	0	0	0	0	0	0	0	1.6
π_0	10	20	10	0	40	70	90	0	90	0	0	0	0	60	100	0	0	0	0	100	100	90	100	0	90	38.8
π_0-FAST	0	0	0	10	0	0	0	0	0	0	0	0	0	0	0	0	0	0	0	0	0	0	0	0	0	0.4
$\pi_{0.5}$	60	80	60	100	100	100	90	20	100	0	40	40	0	100	100	10	10	0	0	100	100	100	100	100	100	64.4
GR00T N1.6	20	30	50	40	0	10	40	0	80	0	0	0	0	80	70	0	0	0	0	70	70	80	80	80	80	35.2
Action-Sketcher	20	40	60	40	80	70	90	0	100	0	0	0	0	90	100	0	0	0	0	100	100	100	100	0	100	47.6
Cosmos Policy	0	0	10	60	30	40	90	0	100	0	0	0	0	100	100	0	0	0	0	100	100	100	100	0	90	40.8
SmolVLA	0	0	0	0	30	0	0	0	10	0	0	0	0	0	0	0	0	0	0	0	0	0	10	0	0	2.0
Dita	0	0	0	0	20	50	10	0	100	0	0	0	0	80	20	0	0	0	0	90	90	50	100	40	90	29.6
RAIN-L	**70**	**80**	**60**	**80**	**60**	**70**	**70**	**50**	**100**	**100**	**50**	**80**	**100**	**100**	**100**	**60**	**40**	**40**	**50**	**100**	**70**	**80**	**100**	**90**	**100**	**76.0**
RAIN-S	**0**	**60**	**60**	**30**	**20**	**0**	**50**	**20**	**80**	**90**	**100**	**90**	**100**	**100**	**100**	**10**	**80**	**10**	**0**	**100**	**60**	**70**	**70**	**30**	**10**	**53.6**

Table 6: **Detailed LIBERO-EX Layout Robustness Results.** Each column is a LIBERO-EX task index from the task-definition tables above. Success rates are reported in % over 10 evaluation episodes, with the category average in the last column.

Model	**Task ID**																									**Avg.**
	026	027	028	029	030	031	032	033	034	035	036	037	038	039	040	041	042	043	044	045	046	047	048	049	050	Avg.
OpenVLA-OFT	0	0	0	0	0	0	0	0	0	0	0	0	0	0	0	0	0	0	0	0	0	0	0	0	0	0.0
π_0	20	50	60	70	40	60	0	50	90	80	60	0	100	0	30	0	10	30	0	100	20	40	0	10	10	37.2
π_0-FAST	10	0	10	0	0	0	0	0	0	0	0	10	0	10	30	20	50	40	20	20	30	60	10	0	0	12.8
$\pi_{0.5}$	70	60	100	100	100	80	40	100	100	90	90	0	100	0	90	0	100	100	0	100	0	10	0	0	0	57.2
GR00T N1.6	0	0	50	40	70	10	0	70	20	70	40	0	80	0	0	10	80	30	50	40	30	40	30	10	10	31.2
Action-Sketcher	10	70	50	90	40	40	0	90	10	100	20	0	30	0	40	10	10	0	0	40	0	30	0	10	0	27.6
Cosmos Policy	10	10	40	100	80	90	10	100	70	40	60	0	100	0	90	0	100	100	0	100	0	60	0	0	50	48.4
SmolVLA	0	0	0	0	0	0	0	0	0	0	0	10	20	0	0	0	10	60	10	20	20	0	0	0	0	6.0
Dita	10	0	0	90	80	90	0	70	30	70	40	0	40	0	10	0	0	40	0	60	0	20	0	0	0	26.0
RAIN-L	**80**	**70**	**90**	**100**	**90**	**100**	**10**	**80**	**90**	**100**	**90**	**100**	**90**	**10**	**80**	**20**	**100**	**100**	**70**	**90**	**60**	**100**	**20**	**50**	**10**	**72.0**
RAIN-S	**20**	**60**	**80**	**90**	**80**	**60**	**30**	**80**	**20**	**40**	**50**	**60**	**70**	**0**	**70**	**0**	**100**	**100**	**50**	**100**	**50**	**90**	**10**	**0**	**40**	**54.0**

Table 7: **Detailed LIBERO-EX Task Comprehension Results.** Each column is a LIBERO-EX task index from the task-definition tables above. Success rates are reported in % over 10 evaluation episodes, with the category average in the last column.

Model	**Task ID**																									**Avg.**
	051	052	053	054	055	056	057	058	059	060	061	062	063	064	065	066	067	068	069	070	071	072	073	074	075	Avg.
OpenVLA-OFT	0	0	0	0	0	0	0	0	0	0	0	0	0	0	0	0	0	0	0	0	0	0	0	0	0	0.0
π_0	0	0	0	0	0	0	0	0	0	0	10	0	20	30	20	0	40	0	10	0	10	0	0	10	0	6.0
π_0-FAST	0	0	0	0	0	0	0	0	0	0	20	40	0	0	0	20	40	0	0	20	10	0	20	0	10	7.2
$\pi_{0.5}$	0	0	0	0	0	0	20	30	0	0	0	0	0	0	0	0	10	0	0	0	0	0	0	0	0	2.4
GR00T N1.6	0	0	0	0	0	0	0	0	0	0	20	10	0	0	0	10	20	0	0	0	10	0	0	0	0	2.8
Action-Sketcher	0	0	0	0	0	0	0	0	0	0	0	0	0	20	10	0	20	0	0	10	10	10	0	0	0	3.2
Cosmos Policy	0	0	0	0	0	0	0	0	0	0	10	0	0	30	0	0	10	0	0	0	0	50	0	40	0	5.6
SmolVLA	0	0	0	0	0	0	0	0	0	0	0	0	0	0	0	0	30	0	0	0	10	0	0	0	10	2.0
Dita	0	0	0	0	0	0	0	0	0	0	20	10	50	10	40	0	20	0	50	0	40	0	0	0	0	9.6
RAIN-L	**10**	**0**	**0**	**20**	**20**	**10**	**20**	**30**	**20**	**20**	**90**	**100**	**100**	**100**	**70**	**90**	**100**	**20**	**50**	**70**	**100**	**70**	**100**	**100**	**20**	**53.2**
RAIN-S	**10**	**0**	**10**	**0**	**30**	**0**	**0**	**40**	**20**	**0**	**80**	**100**	**60**	**90**	**60**	**70**	**100**	**10**	**90**	**100**	**80**	**100**	**100**	**90**	**20**	**50.4**

Table 8: **Object grounding tasks.** Selected initial images for the object grounding category, part 1 of 2.

Image	Task ID	Image Type	Description
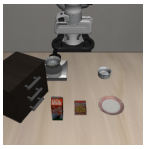	001	Unseen object	Pick the milk next to the cookies box and place it on the plate.
	002	Unseen object	Pick the alphabet soup next to the plate and place it on the plate.
	003	Unseen object	Pick the tomato sauce next to the plate and place it on the plate.
	004	Unseen object	Put the white mug on the stove.
	005	Unseen object	Pick the tomato sauce between the plate and the ramekin and place it on the plate.
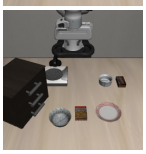	006	Unseen object	Pick the chocolate pudding next to the ramekin and place it on the plate.
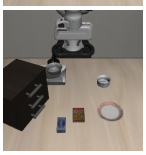	007	Unseen object	Pick the cream cheese next to the cookies box and place it on the plate.
	008	Object switching	Pick the salad dressing and place it in the basket.
	009	Object switching	Pick the milk and place it in the basket.
	010	Object switching	Pick the tomato sauce and place it in the basket.
	011	Object switching	Pick the alphabet soup and place it in the basket.
	012	Object switching	Pick the butter and place it in the basket.
	013	Object switching	Pick the ketchup and place it in the basket.

Table 9: **Object grounding tasks.** Selected initial images for the object grounding category, part 2 of 2.

Image	Task ID	Image Type	Description
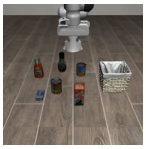	014	Object switching	Pick the tomato sauce and place it in the basket.
	015	Object switching	Pick the cream cheese and place it in the basket.
	016	Object switching	Pick the bbq sauce and place it in the basket.
	017	Object switching	Pick the ketchup and place it in the basket.
	018	Object switching	Pick the tomato sauce and place it in the basket.
	019	Object switching	Pick the orange juice and place it in the basket.
	020	Object switching	Pick the chocolate pudding and place it in the basket.
	021	Object switching	Pick the bbq sauce and place it in the basket.
	022	Object switching	Pick the orange juice and place it in the basket.
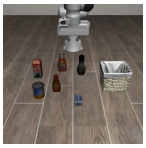	023	Object switching	Pick the milk and place it in the basket.
	024	Object switching	Pick the cream cheese and place it in the basket.
	025	Object switching	Pick the alphabet soup and place it in the basket.

Table 10: **Layout robustness tasks.** Selected initial images for the layout robustness category.

Image	ID	Description	Image	ID	Description
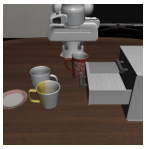	026	Put the white mug on the left plate.		027	Put the white mug on the left plate.
	028	Put the white mug in the basket.		029	Put the white mug on the plate.
	030	Put the white mug on the plate.	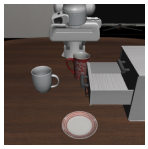	031	Put the white mug on the plate.
	032	Put the chocolate pudding in the basket.		033	Put the white mug on the plate.
	034	Put the white mug on the left plate.		035	Put the white mug on the left plate.
	036	Put the yellow and white mug in the microwave.		037	Close the microwave.
	038	Put the yellow and white mug in the microwave.		039	Close the microwave.
	040	Close the microwave.	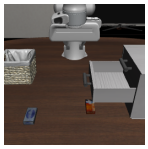	041	Close the middle drawer of the white cabinet.
	042	Turn on the stove.		043	Turn on the stove.
	044	Close the middle drawer of the cabinet.		045	Put the black bowl in the middle drawer of the cabinet.
	046	Close the middle drawer of the cabinet.		047	Close the top drawer of the cabinet.
	048	Close the bottom drawer of the cabinet.		049	Put the yellow and white mug in the microwave.
	050	Turn on the stove.			

Table 11: **Task comprehension tasks.** Selected initial images for the task comprehension category, part 1 of 2.

Image	Task ID	Image Type	Description
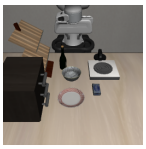	051	Task composition	Put the bowl on the plate, and then open the middle drawer of the cabinet.
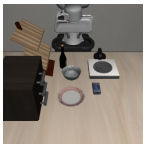	052	Task composition	Put the wine bottle on the rack, and then open the top drawer and put the bowl inside.
	053	Task composition	Put the wine bottle on the rack, and then turn on the stove.
	054	Task composition	Open the top drawer and put the bowl inside, and then put the wine bottle on top of the cabinet.
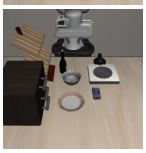	055	Task composition	Open the top drawer and put the bowl inside, and then turn on the stove.
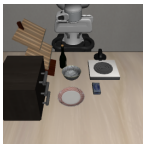	056	Task composition	Put the cream cheese in the bowl, and then put the wine bottle on top of the cabinet.
	057	Task composition	Put the cream cheese in the bowl, and then push the plate to the front of the stove.
	058	Task composition	Put the cream cheese in the bowl, and then turn on the stove.
	059	Task composition	Push the plate to the front of the stove, and then turn on the stove.
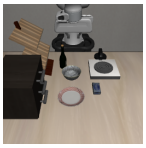	060	Task composition	Turn on the stove, and then open the middle drawer of the cabinet.
	061	Task decomposition	Put the white mug on the left plate.
	062	Task decomposition	Put the yellow and white mug on the right plate.

Table 12: **Task comprehension tasks.** Selected initial images for the task comprehension category, part 2 of 2.

Image	Task ID	Image Type	Description
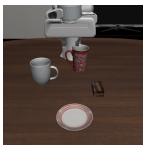	064	Task decomposition	Put the chocolate pudding to the right of the plate.
	065	Task decomposition	Put the yellow and white mug in the microwave.
	066	Task decomposition	Close the microwave.
	067	Task decomposition	Turn on the stove.
	068	Task decomposition	Put the moka pot on the stove.
	069	Task decomposition	Put the alphabet soup in the basket.
	070	Task decomposition	Put the cream cheese box in the basket.
	071	Task decomposition	Put the alphabet soup in the basket.
	072	Task decomposition	Put the tomato sauce in the basket.
	073	Task decomposition	Put the cream cheese box in the basket.
	074	Task decomposition	Put the butter in the basket.
	075	Task decomposition	Close the bottom drawer of the cabinet.

C Real-World Experiment Details

In this section, we provide additional details for the real-world robot experiments, including the robot setup, dataset construction, evaluation splits, and baseline training details.

C.1 Common Setup

Robot platform. Our real-world setup is shown in Fig. 5. We use a ROBOTIS OMY-F3M robot equipped with a 6-DoF manipulator driven by high-precision DYNAMIXEL-Y actuators and a 1-DoF two-finger gripper. For perception, we use three RGB camera viewpoints: an Intel RealSense D405 wrist camera mounted near the end-effector, and two Intel RealSense D435 cameras for the third-person and top-down views.

Control interface. All methods use the same 7-dimensional joint-space policy interface. The robot state consists of six arm joint positions and one gripper joint value, and the policy action consists of six absolute target joint angles and one gripper command. We use absolute joint-pose control instead of end-effector delta control for real-world execution, so the predicted actions can be directly sent to the OMY-F3M joint trajectory controller. The robot client executes joint commands at 30 Hz.

Deployment infrastructure. Robot control is managed by a ROS-based rollout client, while each policy runs as a separate model server on an NVIDIA RTX PRO 6000 workstation. The rollout client reads live camera frames and robot joint states, sends the assembled observation to the selected model server, receives an action chunk, and publishes the predicted joint targets to the robot controller. The client queries the model server asynchronously while executing the current action chunk, allowing policy inference and robot control to run concurrently.

Figure 5: **Real-world experimental setup.** The OMY-F3M robot is observed by wrist, third-person, and top-down RGB cameras and controlled through a 7D joint-absolute action interface.

Real-world dataset. We collect OMY-F3M demonstrations using a ROS-based recorder and store them in the LeRobot format [5]. Each trajectory contains synchronized RGB observations from the wrist, third-person, and top-down cameras, robot joint states, actions, and end-effector poses at 30 Hz. We construct an aggregated real-world dataset from the task-specific datasets. All tasks share the same embodiment, camera setup, state representation, and 7D joint-absolute action space.

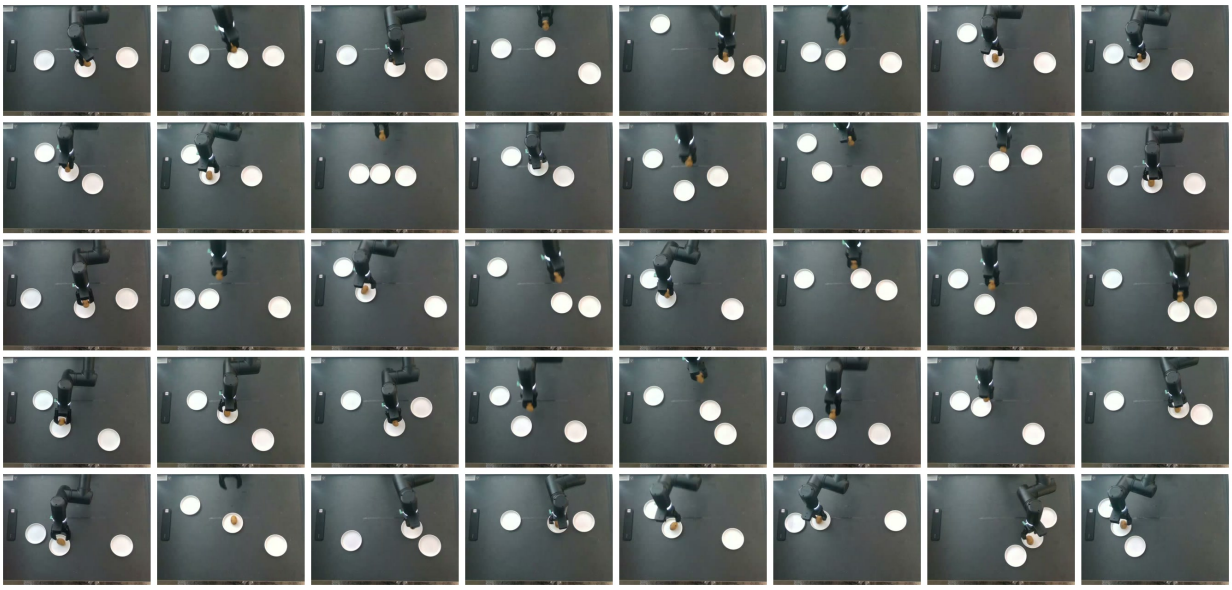

Figure 6: **Qualitative samples from the `Potato-to-Plate` task.** All 40 collected episodes are shown from the top camera, with one representative frame sampled from each trajectory. The grid is ordered row-major by episode index: the horizontal direction advances through consecutive episodes, and the vertical direction continues the episode sequence after each row.

C.2 Real-World Task Suites

Rather than benchmarking on standard, isolated scenarios, our real-world evaluation protocol is explicitly constructed to heavily prioritize out-of-distribution (OOD) generalization within visually and spatially cluttered settings. All methods are trained on identical, data-efficient sets of real-robot demonstrations within each family and evaluated using the same physical platform, camera configuration, action interface, initial-state protocol, and success criteria.

While In-Distribution (ID) trials establish baseline performance, our primary focus lies in these comprehensive OOD evaluation splits. A central objective of these splits is to expose policies to dense, cluttered environments where multiple objects are scattered and reshuffled simultaneously across the workspace. By heavily stacking these variations—spanning permuted relative layouts, completely unseen target categories, and displaced target positions—we force the models to operate in scenes packed with visual distractors. This rigorous, OOD-centric protocol explicitly tests whether a policy possesses the fine-grained visual-spatial reasoning required to segment and ground instruction-relevant regions out of a cluttered scene, or if it collapses under superficial shortcuts memorized from the clean, structured training demonstrations.

To qualitatively summarize the real-world data collection process, we visualize representative frames sampled from the collected demonstrations in Figures 6–7. These visualizations show the range of object layouts, camera viewpoints, and trajectory-level variation used to construct the real-world training datasets.

For visualization, we therefore project object-pose distributions onto the actual camera images and additionally show ROI-focused views that highlight the small manipulation region in which successful actions must be grounded.

C.3 RAIN Real-World Deployment Architecture

To execute long-horizon natural language instructions without control-loop bottlenecks, we deploy our framework using a decoupled serving stack engineered specifically to maximize the throughput of the **Region-Aware Interaction Network (RAIN)**. As schematically illustrated in Figure 9, the system architecture segregates the unconstrained, low-frequency visual-symbolic grounding of general-purpose Vision-Language Models (VLMs) from RAIN's high-frequency visuomotor action generation loop.

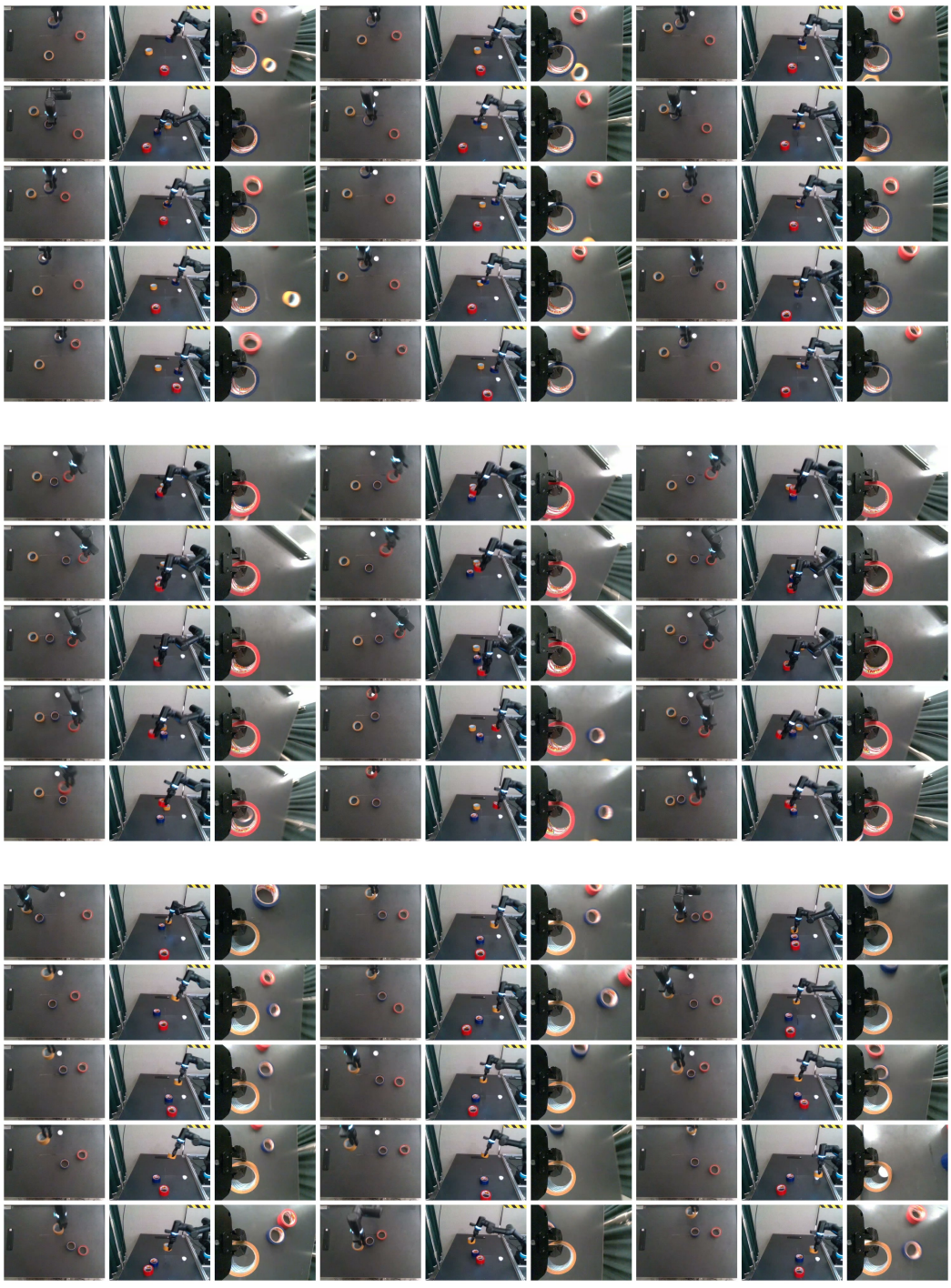

Figure 7: **Qualitative samples from the `Tape-to-Clay` task suite.** The three bands show blue, red, and yellow tape variants, respectively. For each variant, all 15 collected episodes are shown, with columns repeating top, third-person, and wrist camera views. The horizontal direction is organized as episode-wise camera triplets (top/third-person/wrist) for consecutive episodes, while the vertical direction continues the remaining episode groups. The vertical stacking across bands corresponds to the target tape color rather than a physical workspace coordinate.

A central design paradigm of this deployment is that the VLM does not function as a per-frame closed-loop controller, a live completion judge, or an online task planner. Instead, the symbolic instruction decomposition is offloaded onto a structured task registry that specifies the ordered subtasks, target linguistic phrases, and low-level action primitives.

At the temporal boundary of each subtask transition, the live mask server invokes the VLM (`Cosmos-Reason2-2B`) exactly once. The VLM processes the current multi-view observation to ground the active target phrase (e.g., *"the potato"*) into a localized 2D bounding box, which serves as a zero-shot spatial anchor to initialize a high-speed SAM 2 tracking thread. Once initialized, SAM 2 handles token-free mask propagation across subsequent frames, completely removing the heavy VLM inference overhead from the active control loop.

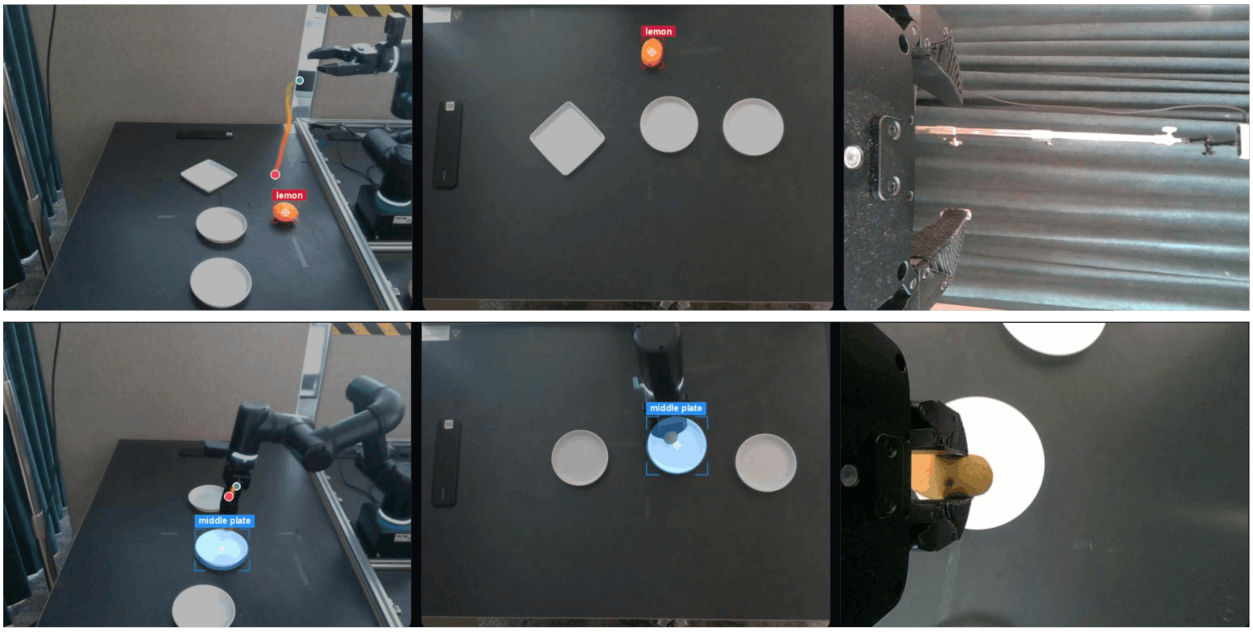

Figure 8: **Real-World Multi-View Setup and Target Grounding Visualization.** Examples of synchronized multi-view observations used in our real-world experiments: third-person, top-down, and wrist camera views. The perception pipeline dynamically initializes a zero-shot 2D bounding box via the VLM (e.g., grounding "middle plate") and propagates the region mask to guide the RAIN motor policy for robust manipulation.

Downstream low-level control is entirely executed by the RAIN motor server at 30 Hz. The RAIN policy consumes multi-view RGB observations, the tracked SAM 2 region masks, and the 7-DoF robot state configured under a strict joint-position and joint-absolute action space contract. By explicitly injecting the tracked masks into RAIN's target-aware visual layers, the policy jointly predicts target-directed action chunks ($H_{\text{action}} = 16$, $H_{\text{execute}} = 10$) and an auxiliary task-completion (TC) score. Sequential subtask switching is triggered autonomously by RAIN's internal progress-estimation head (tc ≥ 0.7 over consecutive frames) or manually overridden via the operator dashboard. Upon a transition signal, the client advances the registry pointer, dynamically flashing the next target phrase to re-initialize the VLM bounding box grounding cycle.

Interactive mask retargeting. To further verify that RAIN uses the region mask as an actionable conditioning signal, we evaluate an interactive click-to-act mode. In this mode, the operator selects a target region directly from the live dashboard by clicking on the camera stream. The click initializes a SAM 2 point-prompt mask for the selected connected component, and the resulting mask is sent to RAIN through the exact same interface used during autonomous operations. The policy checkpoint, robot state interface, action space, and active action type remain completely unchanged; only the target region mask is dynamically altered.

This setup provides a rigorous causal test of region conditioning. For example, during a placement subtask, the operator can click different candidate plates or target objects within the same scene. When the clicked

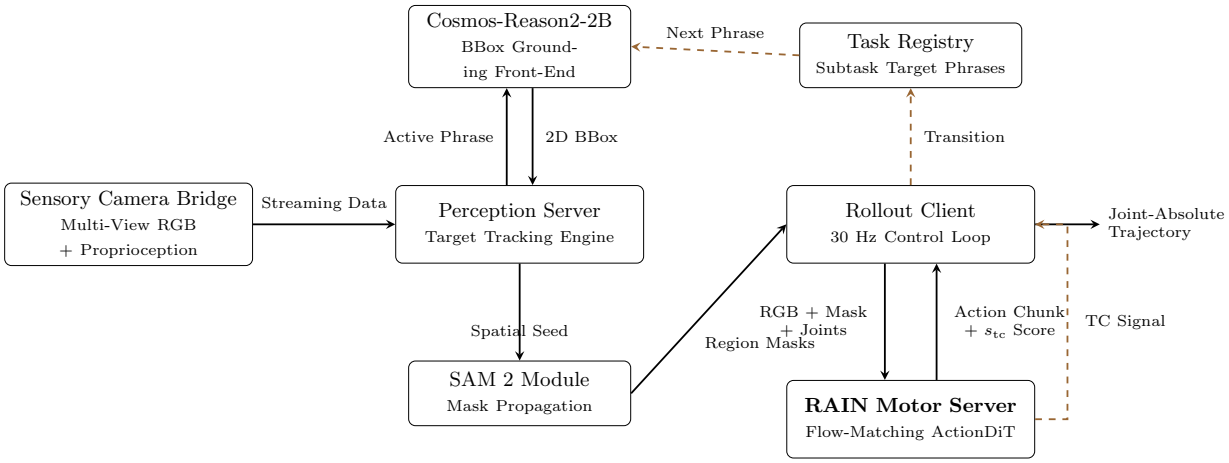

Figure 9: **RAIN Real-World Serving Pipeline.** The architecture explicitly separates sparse vision-language target initialization from closed-loop control. At each subtask boundary, the VLM grounds the registry phrase into a 2D bounding box to seed SAM 2 tracking. The resulting region masks are directly consumed by the **RAIN motor server** alongside multi-view RGB observations to generate joint-absolute action chunks and drive autonomous progress estimation.

mask changes from one target region to another, RAIN dynamically retargets the predicted end-effector trajectory and the executed placement behavior toward the newly selected region in real-time. Similarly, during a grasp subtask, clicking a different valid source object changes the grasp target while preserving the underlying low-level grasp primitive.

Protocol. We keep the scene, robot checkpoint, task family, and action interface entirely fixed across all interactive evaluations. For each trial, we manually select the active subtask from the dashboard, e.g., `grasp` for source-object selection or `place` for placement-target selection. We then click a target region in the live camera stream to initialize a SAM 2 mask. The rollout client receives this clicked mask exactly as it receives an autonomous VLM-grounded mask. We compare the emergent trajectories across different clicked regions while keeping all other inputs fixed. A successful retargeting trial is counted when the robot correctly executes the intended primitive toward the clicked region, such as grasping the specific clicked object or placing the held object onto the newly designated target.

C.4 Real-World Baseline Training Details

We fine-tune all baseline policies on the same real-world demonstrations used by RAIN. For each method, we use the released pretrained checkpoint and official fine-tuning code when available, and adapt only the input/output interface to the OMY-F3M setting. In particular, each baseline receives the same three RGB camera views, language instruction, and 7D robot state, and outputs actions through the same 7D joint-absolute action interface. RAIN additionally receives online masks for the third-person and top-down views; baselines do not receive these mask-conditioning inputs. The detailed training configurations and hyperparameter settings for all evaluated models are summarized in Table 13.

C.4.1 MolmoAct2

We adapt MolmoAct2 [7] using the released LeRobot-style policy implementation, initialized from the public MolmoAct2 checkpoint.[1] We use this checkpoint because it is the closest released MolmoAct2 initialization to our real-world setting: SO-100/101 and OMY-F3M are both tabletop single-arm manipulation embodiments controlled with continuous joint-space action trajectories, although their kinematics and action dimensions differ.

[1] Allen AI MolmoAct2. `https://huggingface.co/allenai/MolmoAct2-SO100_101`

Table 13: **Hyperparameters for OMY-F3M real-world finetuning.** All methods are trained on the same OMY-F3M teleoperation trajectories, utilizing 3 camera views (third-person, top-down, wrist) and 7 DoF absolute joint-pose control.

Setting	GR00T N1.6	X-VLA	MolmoAct2	RAIN (Ours)
Base & shared settings				
Base model	GR00T-N1.6-3B	X-VLA-0.9B	MolmoAct2-SO100	DINOv2 ViT-L/14 + DiT
# GPUs	1	1	1	2
Learning rate	1e−4	1e−4	1e−5/5e−5*	1e−4
LR schedule	cosine (wu 0.05)	wu 2k	cosine (wu 0.05)	wu 2k
Total batch size	8	8	8	32
Grad. accum.	1	4	1	1
Weight decay	1e−5	–	1e−5	0.01
Optimizer	AdamW	AdamW	AdamW	AdamW
Precision	bf16	bf16	bf16	bf16
Image input	3 views	3 views	3 views (480×640)	3 views (DINO 448)
Use proprio	yes	yes	yes	yes
Action chunk	16	32	16	16
Method-specific settings				
Finetune scope	proj.+VLLN+DiT+top-4 LLM	soft-prompt PEFT	VLM + action expert	full FT (FiLM)
% trainable param	1.62B (49.3%)	∼1%	partial	full
Denoising steps	4	10	8	4
Extra conditioning	–	32-dim domain prompt	–	SAM2 mask + 8 plan wp

For OMY-F3M, we adapt the embodiment metadata, dataset interface, state/action dimensionality, and rollout adapter to the 6-DoF arm plus 1-DoF gripper. The observation contains the same three RGB camera views, language instruction, and 7D proprioceptive state used by the other real-world methods.

During fine-tuning, we freeze the Molmo2-derived vision-language backbone, including the vision encoder, vision-language connector, language model, and token embeddings. We train only the continuous action expert, adapting the SO-100/101 action distribution to the OMY-F3M 7D joint-absolute action space. This keeps the visual-language representation fixed and limits trainable capacity for the small real-robot datasets. The adapted policy predicts a 16-step action chunk $a_{t:t+15} \in \mathbb{R}^{16\times 7}$, where each action consists of six absolute arm-joint targets and one gripper command. The shared rollout client executes these joint-absolute commands at 30 Hz.

C.4.2 X-VLA

We fine-tune X-VLA [41] from the public X-VLA checkpoint[2] The model is adapted to the same OMY-F3M LeRobot demonstrations used by all real-world methods, with three RGB views, a language instruction, a 7D robot state, and a 7D joint-absolute action.

X-VLA uses a padded cross-embodiment action interface. We set `action_mode=auto`, `real_action_dim=7`, and `max_action_dim=20`. The first seven dimensions correspond to the OMY-F3M action space, consisting of six arm joint targets and one gripper command, while the remaining dimensions are dummy padded channels. The training loss is applied only to the valid 7D action dimensions, and inference outputs are trimmed back to 7D before execution.

We fine-tune X-VLA with PEFT/LoRA adapters using rank 8 and alpha 16. The base pretrained weights remain frozen, while the LoRA adapters, domain soft prompt, and action encoder/decoder components are saved in the adapter checkpoint. We train with AdamW, learning rate 1×10^{-4}, 2k warmup steps, bfloat16 precision, global batch size 8, and gradient accumulation 4.

At deployment, X-VLA is served through the same ZMQ rollout interface as the other baselines. The policy receives the current multi-view observation, proprioceptive state, and instruction, then returns a 7D joint-absolute action chunk to the 30 Hz rollout client.

[2]X-VLA Official Checkpoints. `https://huggingface.co/collections/2toINF/x-vla`,

C.4.3 GR00T N1.6

We fine-tune GR00T N1.6 [26] using the released Isaac GR00T post-training codebase, initialized from the public GR00T-N1.6-3B checkpoint[3]. We adapt its embodiment metadata and modality schema to OMY-F3M. The observation contains three RGB views (`cam_wrist`, `cam_third`, and `cam_top`), a language instruction, and a 7D robot state. The state and action are grouped into a 6D `single_arm` joint group and a 1D `gripper` group. Both are registered as joint-space, absolute-action modalities, matching the real-robot joint-position controller.

During fine-tuning, we freeze the visual encoder and do not fully fine-tune the language backbone. We train the action-head projector, the VL-to-latent module, the diffusion action model, and the top four language-model layers, corresponding to approximately 1.62B trainable parameters (49.29%). The action head is trained with conditional flow matching and uses four integration steps at inference.

We train with AdamW, learning rate 1×10^{-4}, cosine decay with warmup ratio 0.05, weight decay 1×10^{-5}, bfloat16 precision, and global batch size 8. The adapted policy predicts action chunks of shape 16×7, consisting of six absolute arm-joint targets and one gripper command. The shared rollout client executes a prefix of each chunk at 30 Hz and then re-queries the policy for closed-loop replanning.

[3]NVIDIA GR00T-N1.6-3B. `https://huggingface.co/nvidia/GR00T-N1.6-3B`